Data examples of logarithm Fourier-domain bidirectional deconvolution

Qiang Fu, Yi Shen and Jon Claerbout

ABSTRACT

Time-domain bidirectional deconvolution methods show great promise for overcoming the minimum-phase assumption in blind deconvolution of signals containing a mixed-phase wavelet, such as seismic data. However, time-domain bidirectional methods usually suffer from slow convergence (Slalom method) or the starting model (Symmetric method). Claerbout proposed a logarithm Fourier-domain method to perform bidirectional deconvolution. In this paper, we test the new logarithm Fourier-domain method on both synthetic data and field data. The results demonstrate that the new method is more stable than previous methods and that it produces better results.

INTRODUCTION

Usually, a seismic data trace d can be defined as a convolution of a wavelet w with a reflectivity series r. This can be written as $d = r * w$, where $*$ denotes convolution. Blind deconvolution seeks to estimate the wavelet and reflectivity series using only information contained in the data. Traditionally, seismic blind deconvolution has two assumptions, namely whiteness and minimum phase. The whiteness assumption supposes that the reflectivity series r is a flat spectrum, while the minimum-phase assumption supposes that the wavelet w is causal and has a stable inverse. Recently, some new methods have been proposed to avoid or correct these two assumptions in seismic blind deconvolution.

In Zhang and Claerbout (2010a), the authors proposed to use a hyperbolic penalty function introduced in Claerbout (2009) instead of the conventional L2 norm penalty function to solve the blind deconvolution problem. With this method, a sparseness assumption replacese of the traditional whiteness assumption in the deconvolution problem. Furthermore, Zhang and Claerbout (2010b) proposed a new method called "bidirectional deconvolution" in order to overcome the minimum-phase assumption. Bidirectional deconvolution assumes that any misxed-phase wavelet can be decomposed into a convolution of two parts: $w = w_a * w_b$, where w_a is a minimum-phase wavelet and w_b is a maximum-phase wavelet. To solve this problem, we estimate two deconvolution filters, a and b, which are the inverses of wavelets w_a and w_b, respectively. Since Zhang and Claerbout (2010b) solve the two deconvolution filters a and b alternately, we call this method the slalom method. Shen et al. (2011a) proposed

another method to solve the same problem. They use a linearized approximation to solve the two deconvolution filters simultaneously. We call this method the symmetric method. Fu et al. (2011) proposed a way to choose an initial solution to overcome the local-minima problem caused by the high nonlinearity of blind deconvolution. Shen et al. (2011b) discuss an important aspect of any inversion problem, preconditioning and how it improves bidirectional deconvolution.

All of the forementioned methods solve the problem in the time domain. Claerbout et al. (2011) proposed a method to solve the problem in the Fourier domain. We will show in a later section that this new method converges faster and is less sensitive to the starting point or preconditioner than the above-mentioned time-domain methods.

METHODOLOGY

Claerbout et al. (2011) show the complete derivation of the method. Here, we describe only the major steps of this method. As with any iterative method, we have two issues to solve in one iteration: the update direction and the step length of the update. Below, we disscuss how we can solve these two issues in the logarithm Fourier-domain method.

As we discussed in the previous section, we can decompose the arbitrary data d into three parts: the reflectivity series r, the minimum phase wavelet w_a and the maximum phase wavelet w_b:

$$d = r * (w_a * w_b). \tag{1}$$

We wish to solve for the deconvolution filters a and b, which should be the inverses of wavelets w_a and w_b:

$$\begin{cases} w_a * a = \delta(n) \\ w_b * b = \delta(n) \end{cases}. \tag{2}$$

From equation 2, we know that a is minimum phase and b is maximum phase. If we know the deconvolution filters a and b, we can get reflectivity series r as follows:

$$r = d * a * b. \tag{3}$$

Next we transform our problem into the Fourier domain. We use capital letters to denote variables in the Fourier domain:

$$R = DAB. \tag{4}$$

We use U to denote the logarithm of the product of A and B:

$$U = \log(AB). \tag{5}$$

Our problem then becomes

$$R = De^U, \tag{6}$$

where U has become our new unknown in bidirectional deconvolution, and we want to update it in each iteration. After some derivation (Claerbout et al., 2011), we get, in the time domain,

$$\begin{cases} \Delta u = r^{\circledast}\mathrm{Hyp}'(r) \\ \Delta r = r * \Delta u \end{cases}, \tag{7}$$

where $^{\circledast}$ means cross-correlation and $\mathrm{Hyp}(r_i) = \sqrt{r_i^2 + R_0^2} - R_0$ is the hyperbolic penalty function.

By Newton's method (using the only first 2 terms of the Taylor expansion), we can calculate the step length α:

$$\alpha = \frac{\sum_i \mathrm{Hyp}'(r_i)\Delta r_i}{\sum_i \mathrm{Hyp}''(r_i)\Delta r_i^2}. \tag{8}$$

Because we use Newton's method, this step length α calculated above is not the final value. To obtain the final step length at each iteration, we need another iteration (nested or second-order iteration):

$\alpha_j = 0$
Iterate(j)
$\quad \alpha_j = \dfrac{\sum_i \mathrm{Hyp}'(r_i)\Delta r_i}{\sum_i \mathrm{Hyp}''(r_i)\Delta r_i^2}$
$\quad \alpha_{final} = \alpha_{final} + \alpha_j$
$\quad r = r + \alpha_j \Delta r$
$\quad u = u + \alpha_j \Delta u$

Given the update directions (both for the unknown u and for the residual r) and the step length α of the update, we have everything we need for each iteration. We can iterate to convergence.

Trial and error on step length α

Because the method above can lead to over-shooting on the step length α, it may lead to a blow-up problem. The Newton method requires a convex function, but for some field data sets that condition may not be met. To overcome this, we use trial and error to avoid step length α being too large. If the hyperbolic penalty function on new $r = r + \alpha\Delta r$ is greater than on original r, the step length α is too large, and we overshoot; in that case, we reduce the step length α by half until the stability

condition is met.

$\alpha_j = 0$
Iterate(j)
$\alpha_j = \dfrac{\sum_i \text{Hyp}'(r_i)\Delta r_i}{\sum_i \text{Hyp}''(r_i)\Delta r_i^2}$
Iterate
If Hyp$(r + \alpha_j \Delta r) <=$ Hyp(r) Then Break
$\alpha_j = \alpha_j / 2$
$\alpha_{final} = \alpha_{final} + \alpha_j$
$r = r + \alpha_j \Delta r$
$u = u + \alpha_j \Delta u$

EXAMPLES

In this section we will test the logarithm Fourier-domain method with both synthetic and field applications. As prior experience shows (Shen et al., 2011b), preconditioning is a critical part of the seismic blind deconvolution problem. Here, we use the Burg Prediction Error Filter (PEF) as the preconditioner for all tests. Unless otherwise specified, we will use one filter for all traces.

In the implementation of the logarithm Fourier-domain method, we use the steepest descent method to search the solution, and for the time domain symmetric method, we use the conjugate direction method. Because of this difference, the convergence speed or the number of iterations required for convergence may not be compared directly.

Synthetic 1D example

First, we demonstrate the advantage of the logarithm Fourier-domain method over the time-domain method on a very simple synthetic data example. The input is a Ricker wavelet generated by an approximate approach that applies a second-order derivative to binomial coefficients (Fu et al., 2011). Figure 1(a) shows a synthetic Ricker wavelet, and 1(b) shows the Ricker wavelet after Burg PEF preconditioning. Next we use the symmetric method (Shen et al., 2011a) to perform time-domain bidirectional deconvolution. Figures 1(c) and 1(d) compare the results of bidirectional deconvolution using the two methods.

For this simple 1D synthetic example, we use 0.1 (which is 5% of the peak amplitute of the input) as the threshold of the hyperbolic penalty function for the logarithm Fourier-domain method and use 95% quantile of the data residual as the threshold for the time-domain method. Using the logarithm Fourier-domain method, we turn the Ricker wavelet into a spike output after about 50 iterations. Using the time-domain

symmetric method, even after 30,000 iterations, we get a major spike followed by a minor spike, plus a few additional jitters at the begining of the trace. At the time of this publication, we do not fully understand why the symmetric method, which utilizes a conjugate direction solver, is significantly slower than the logarithmic method, which utilizes a steepest descent algorithm.One possible explanation, which has not been tested, is that the deconvolution filters derived from the time domain symmetric method are not strictly minimum and maximum phase wavelets.

Another important observation from this synthetic test case is the output location of the bidirectional deconvolution. If we check the wiggles carefully, we can measure that the major peaks of the two deconvolution results in figures 1(c) and 1(d) (both of which are at time sample 104) are not the same as the location of the major peak of the input data figure 1(a) (which is at the time sample 100). Instead, they are located at the major peak location of the preconditioning result in figure 1(b). This inspired us to realize that the output spike location of the deconvolution is determined by the preconditioner, and that we can change the preconditioner to move the spike of the deconvolution result to the location desired. In another paper (Shen et al., 2011b), we discuss this interesting topic in more detail.

Field data common-offset gather example

Now we test the logarithm Fourier-domain bidirectional deconvolution with a 2D marine common offset gather data set that is commonly used to test the time-domain bidirectional deconvolution methods. This 2D marine common-offset gather is very popular in papers discussing blind deconvolution using the hyperbolic penalty function. In Zhang and Claerbout (2010a), Zhang and Claerbout (2010b), Fu et al. (2011), Shen et al. (2011a) and Shen et al. (2011b) the authors tested their methods and theories with this data set as a field data example. Hence this is a good choice for comparing this new method with previous ones.

Figure 2 shows the 2D marine common offset gather. Figure 3 shows the common-offset section after Burg PEF preconditioning. Figures 4 and 5 compare the results of two methods of bidirectional deconvolution.

Figures 6(a) and 6(b) show the comparison of the estimated wavelets from the two methods. Recall that the estimated wavelet is the inverse deconvolution filter. We get the inverse filter by inverting the frequency spectrum of the filter in the Fourier domain, so the wavelet waveform is periodic. This means the jitter we see at the end of the wavelet is the anti-causal part of the filter.

From figures 4 and 5, both methods provide good quality results. However we think the logarithm Fourier-domain method (figure 4) is a little better. First, there are fewer precursors in the the logarithm Fourier domain result than in the time domain result. And the precursor of the logarithm Fourier-domain result does not have a sharp boundary as the precursor of the time domain result. The sharp boundary of the time domain result is caused by the anti-causal deconvolution filter b, which is 20

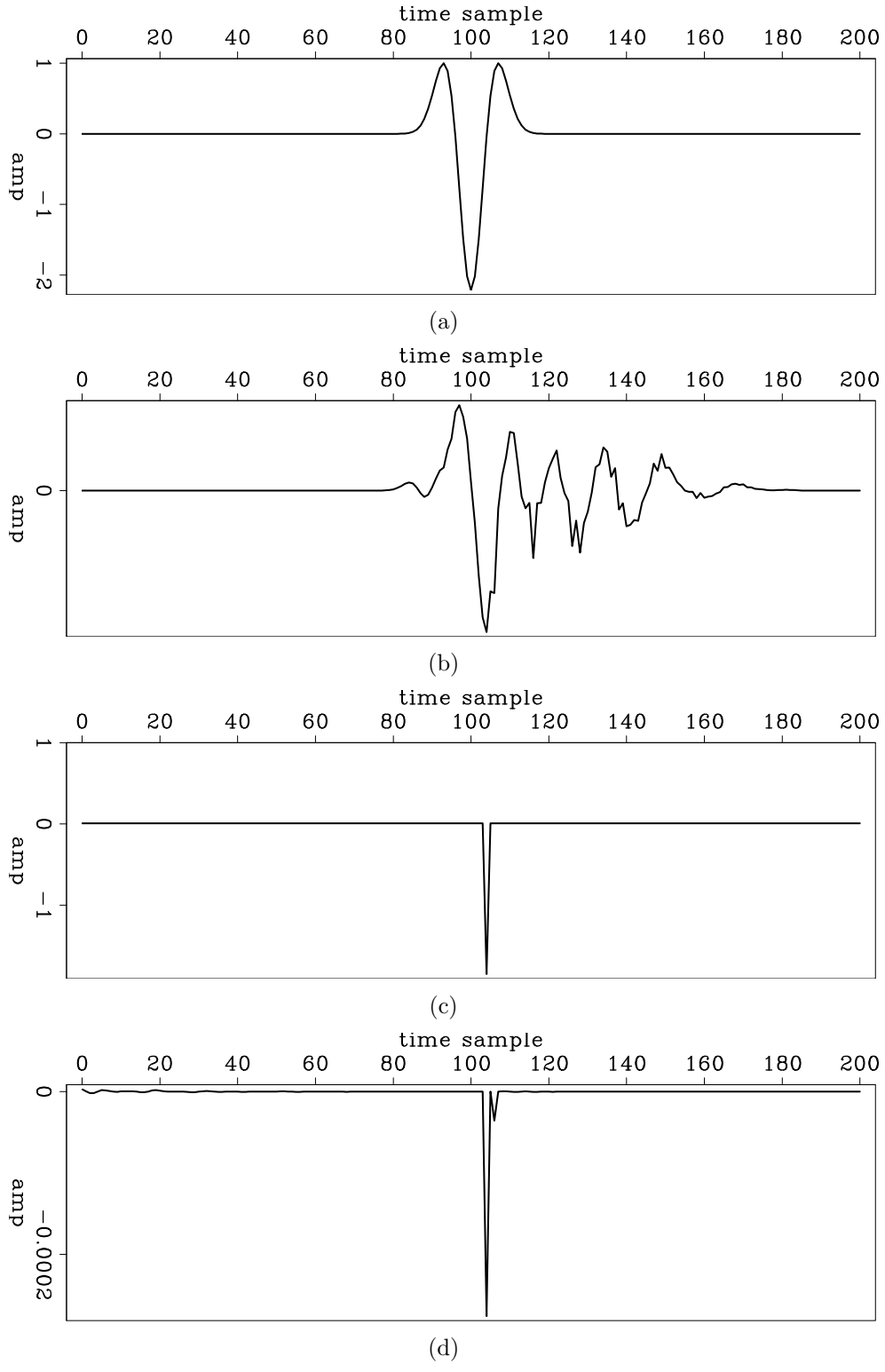

Figure 1: (a) The synthetic Ricker wavelet; (b) The Ricker wavelet after Burg PEF preconditioning; (c) The bidirectional deconvolution result of the logarithm Fourier-domain method after 50 iterations; (d) The bidirectional deconvolution result of the time-domain symmetric method after 30,000 iterations. [**ER**]

sample long, and a sharp boundary on the beginning of the anti-causal deconvolution filter b. Because the logarithm Fourier-domain uses a periodic deconvolution filter, the anti-causal part of the deconvolution filter has no beginning. Moreover, within the salt body (in the vicinity of 2.4 s to 2.6 s), the Fourier-domain result looks cleaner. We find within the salt body, there are fewer low frequency events (which can be seen as the white stripe in figure 5 within 2.4 s to 2.6 s). We do not expect to see any features within the salt body, therefore all events we see in this area in the raw data are the air-gun bubbles. This indicates that the Fourier-domain deconvolution handles the air-gun bubbles better than the time-domain method. However, excluding these differences, the results are similar. We can also find that, except for the tail parts, the estimated wavelets (figures 6(a) and 6(b)) are similar. At the tail of the wavelet which, because of periodicity, correspond to the anticausal part of the logarithm Fourier domain wavelet the wavelet estimated by the time domain symmetric method has less jitter. On the contrary, the logarithm Fourier-domain wavelet appears to have a small anti-causal air-gun bubble.

Here, we have a paradox. From the comparison of deconvolution result (figures 4 and 5), we conclude that in terms of quality, the the logarithm Fourier-domain method is better. But from the wavelet comparison, we can reach an oppsite conclusion. This is because the deconvolution filter in the logarithm Fourier-domain method is periodic and the length of anti-causal part has not an extra constraint, whereas the anti-causal filter in the time domain symmetric method is constrained by the anti-causal filter length parameter and tends to have less anti-causal jitter in the final estimated wavelet.

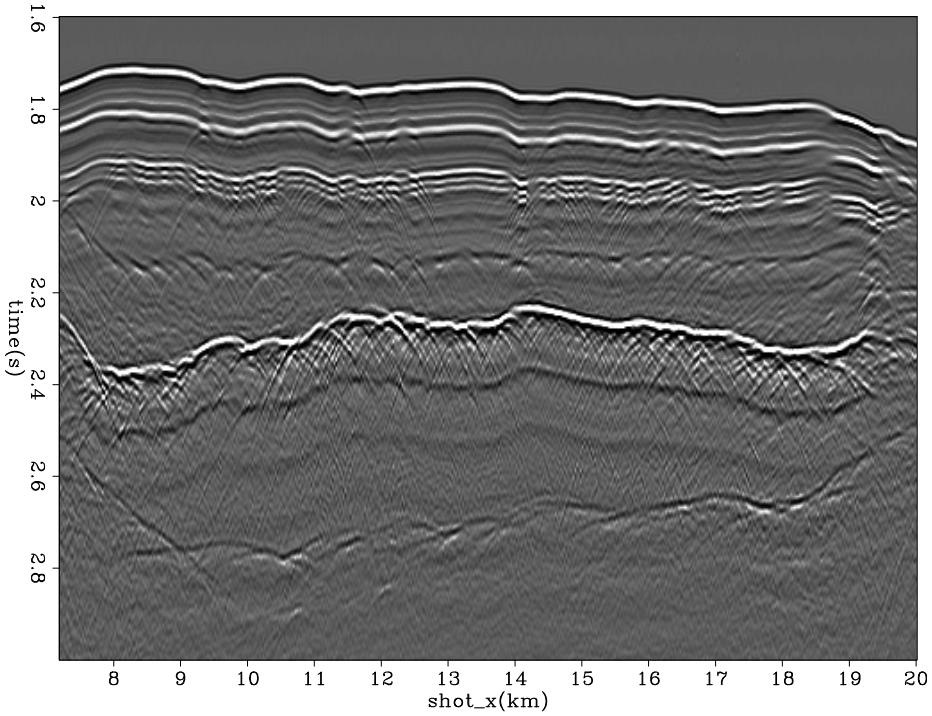

Figure 2: A common-offset section of a marine survey. [**ER**]

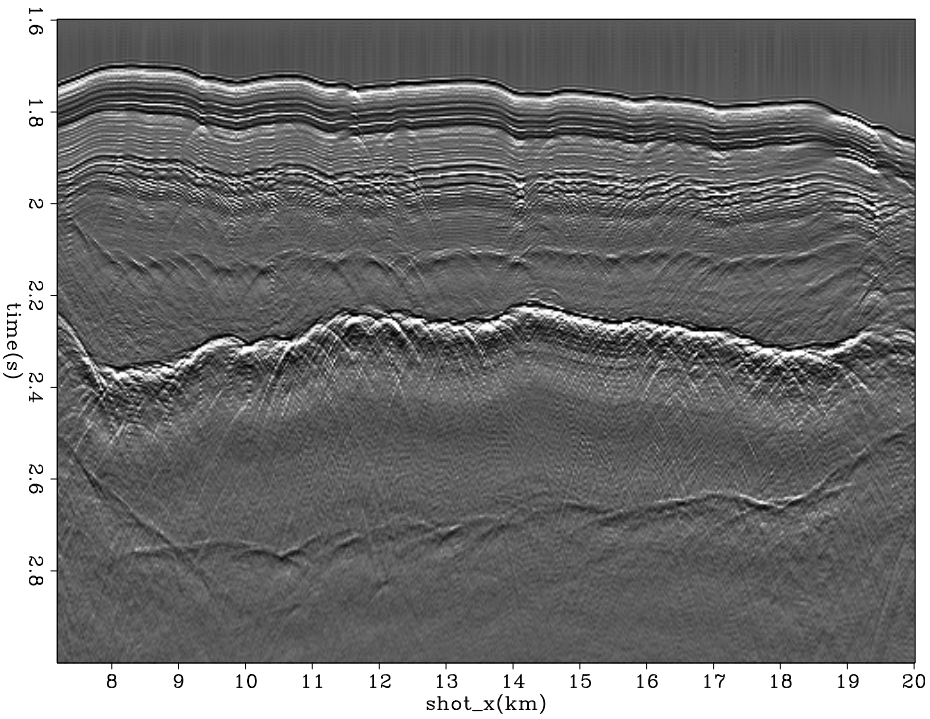

Figure 3: The common-offset section after applying the Burg PEF preconditioner. [**ER**]

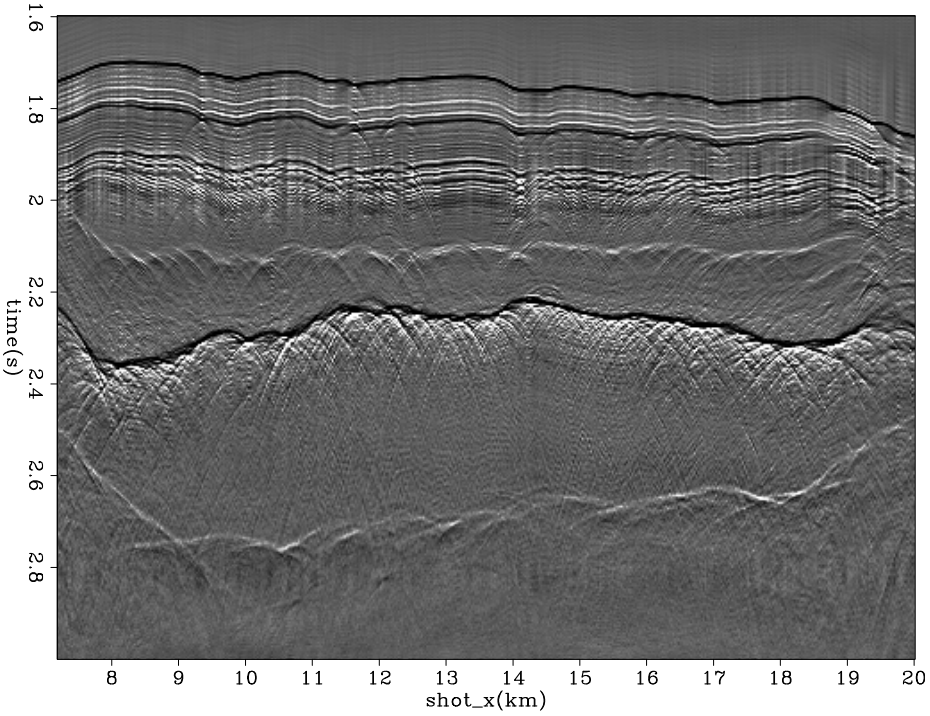

Figure 4: Logarithm Fourier-domain bidirectional deconvolution result. [**ER**]

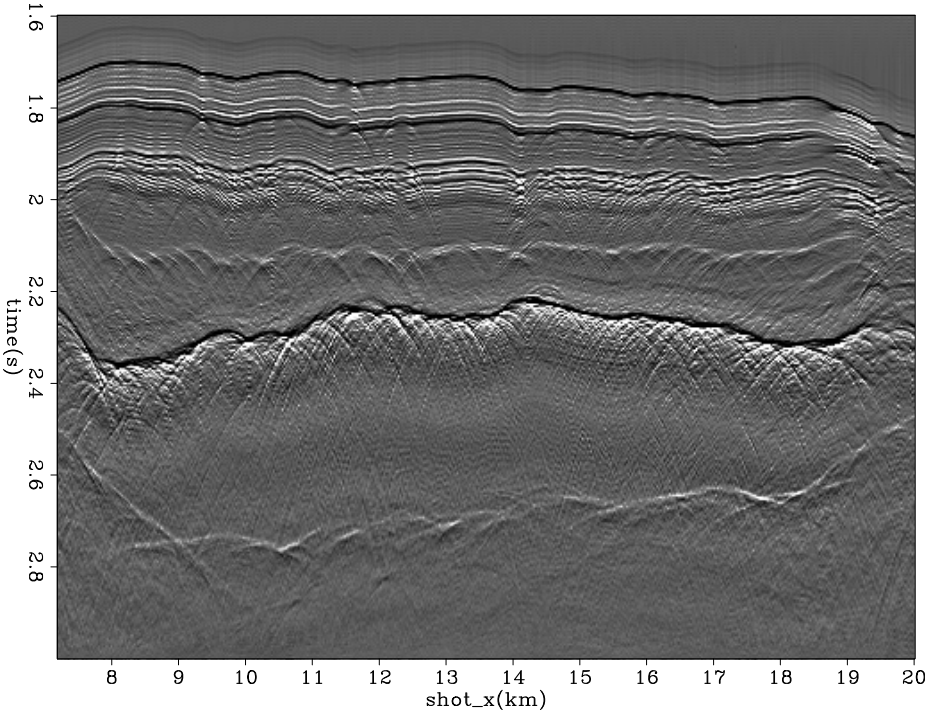

Figure 5: Time-domain (symmetric) bidirectional deconvolution result. [**ER**]

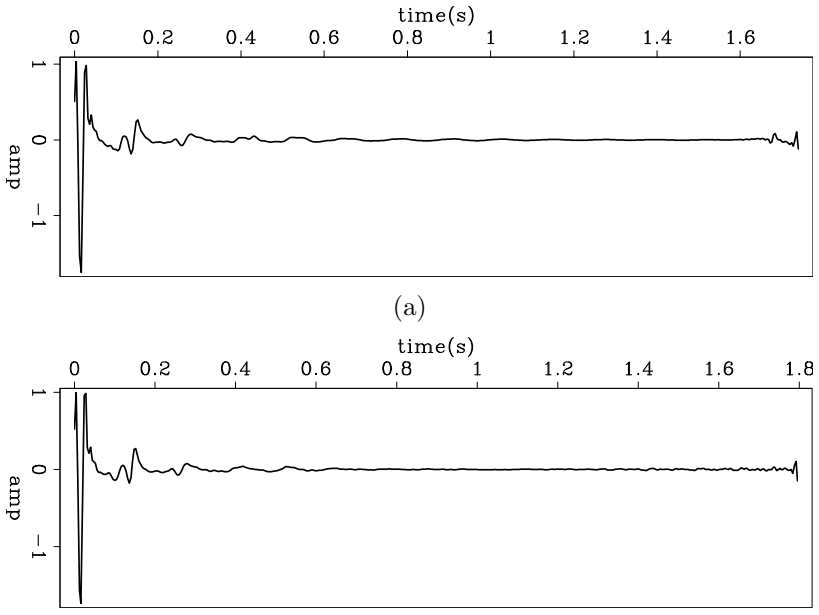

Figure 6: Estimated wavelet from (a) logarithm Fourier-domain and (b) time-domain (symmetric) bidirectional deconvolution. The estimation wavelets are the inverse deconvolution filters, calculated by inverting the frequency spectrum of the filter in the Fourier domain. Therefore the wavelet waveform is periodic, and the jitter we find at the end of the wavelet is the anti-causal part of the filter.

CONCLUSIONS

We test the logarithm Fourier-domain method using both synthetic and field data sets. The results show that this Fourier-domain method has advantages over previous time-domain methods, for both the convergence speed and the quality of the result.

FUTURE WORK

As we mentioned, the 2D marine common offset gather data we used in previous example section has been widely used in judge the result of hyperbolic penalty function based bidirectional deconvolution methods. Because this is the only data set tested so far, conclusions drawn from it are limited. Therefore, we intend to test our methods on other data sets. Next, we discuss some of our preliminary results.

Preliminary Field data pre-stack shot gathers deconvolution result

The common-offset data set we used in previous example section is extracted from a pre-stack survey line. Figure 7 shows the pre-stack shot gathers for the whole survey line. In order to see clearly the deep feature, we use a gain function of t^3 on figure 7. This gain function is only applied here for display purposes here and figure 8 shows two shot gathers in this survey without any gain applied. We also need gain function for deconvolution procedure to ensure the early time and late portion of data have the same weight to contribute to the solution. But We did not figure out what is a suitable gain function of this data set for deconvolution, so in the later test case, we use no gain function in deconvolution procedure.

We find that the previous common-offset gather windowed the data not only in space but also in time. We want to get the data within the same time window as the previous common offset gather. But now we are working on the prestack gathers, and simply cutting a horizontal time window will lose the far-offset part of the deep event, due to the moveout. We do not preform a Normal Move Out correction (NMO) to correct the moveout, because we do not want the stretch caused by NMO to damage the shot waveform. Instead, we perform a constant time shift on each trace and try to flat one target event only. We use a major event in the desired time window, which is the reflection from the top of the salt body, as a target event to calculate the shift time. The shift time fucntion is

$$\tau(x) = t - \sqrt{t_0^2 - x^2/v_0^2}, \tag{9}$$

where x is the offset, v_0 is a constant RMS velocity, t is the travel time at x offset of the target event and t_0 is the travel time at zero offset of the target event. The only unknow in equation 9 is v_0. We can estimated v_0 by picking several points on the target event and do a regression. The Figure 9(a) shows the time-shift function

to flatten the shot gather. We apply this time shift and then window the data set by time window 1.6 s to 3 s, figures 9(b) and (c) show two gathers after this window.

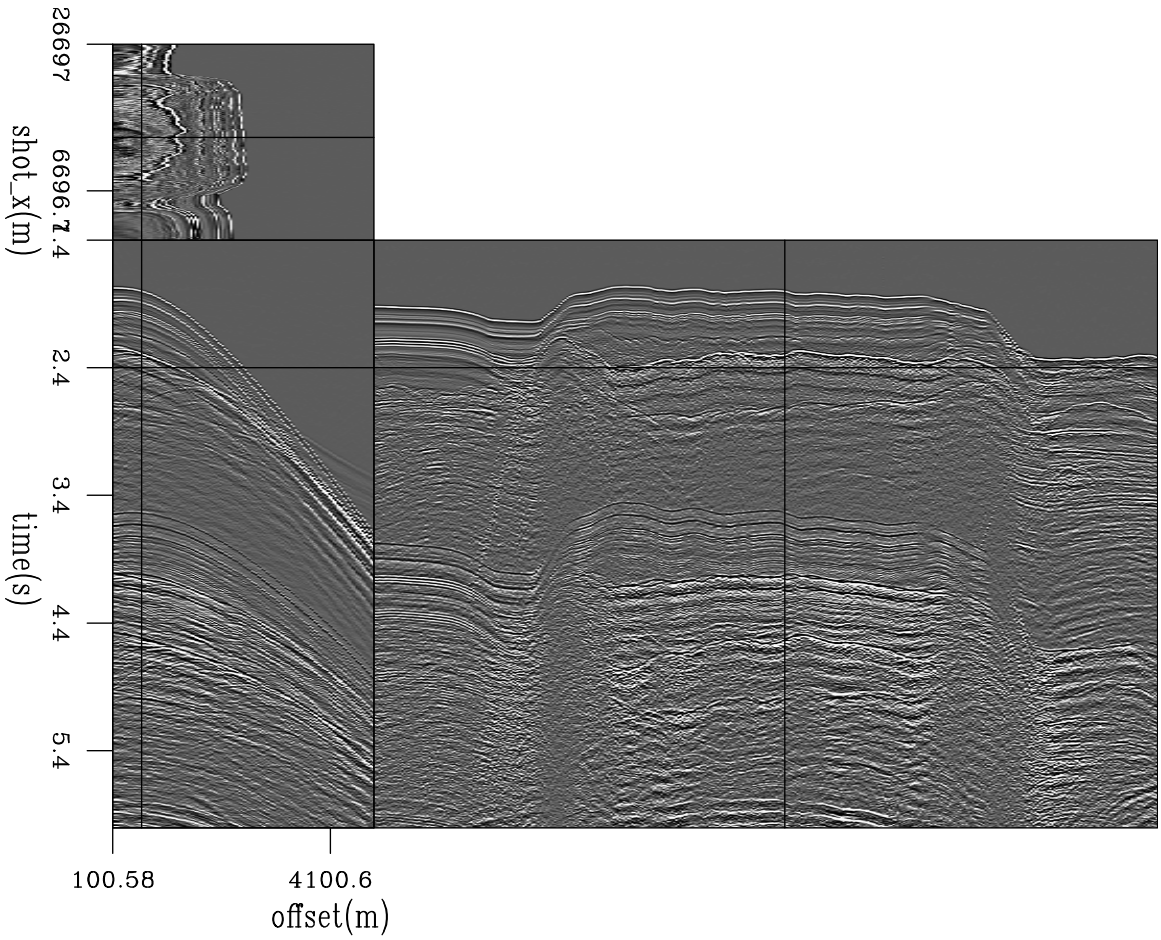

Figure 7: Whole marine pre-stack survey line. [**ER**]

After we get the two windowed shot gathers, we apply the Burg PEF as the preconditioner and then perform the logarithm Fourier-domain bidirectional deconvolution on the two windowed shot gathers. Figure 10 shows the preconditioner results, and figure 11 shows the deconvolution results for the two shot gathers. The two shot gathers are processed independently, which means we use different Burg PEFs and different deconvolution filters on the two shot gathers.

The major event (in the vicinity of 2.2 s), which is the top of the salt body, has a phase shift with increasing offset. In figure 11, the near-offset part of this event is black, and then it turns white after an offset of about 1500 meters. The head wave starts at the same offset of 1500 meters. This is not coincidence, but occurs because the reflection has a 90° phase shift after the critical angle.

Figures 12(a) and 12(b) show the estimated wavelets of these two shot gathers. We see that these are quite similar, indicating that the shot waveforms do not change much between these two shots.

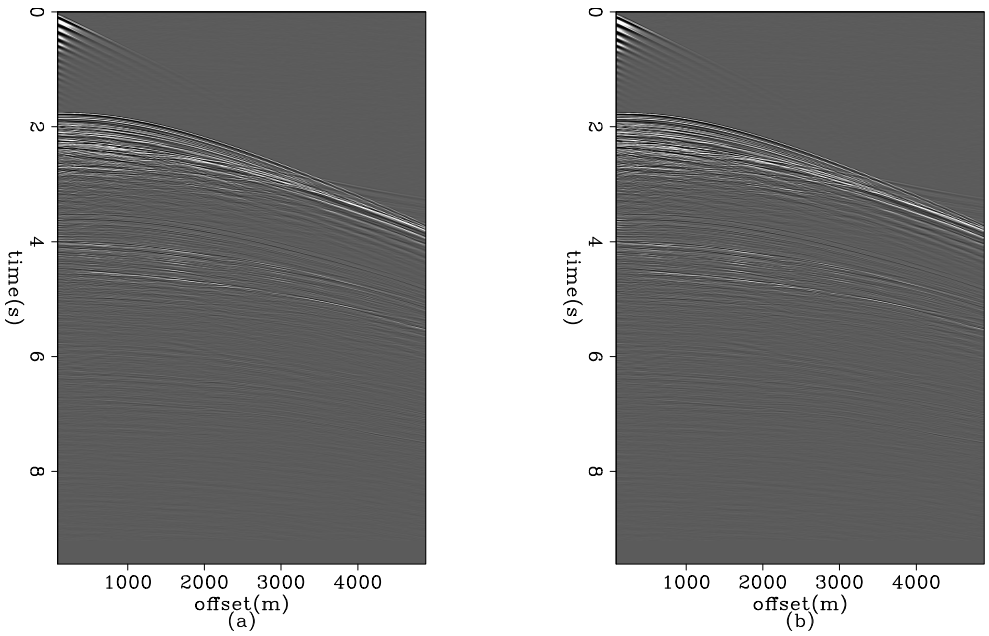

Figure 8: Two shot gathers. [**ER**]

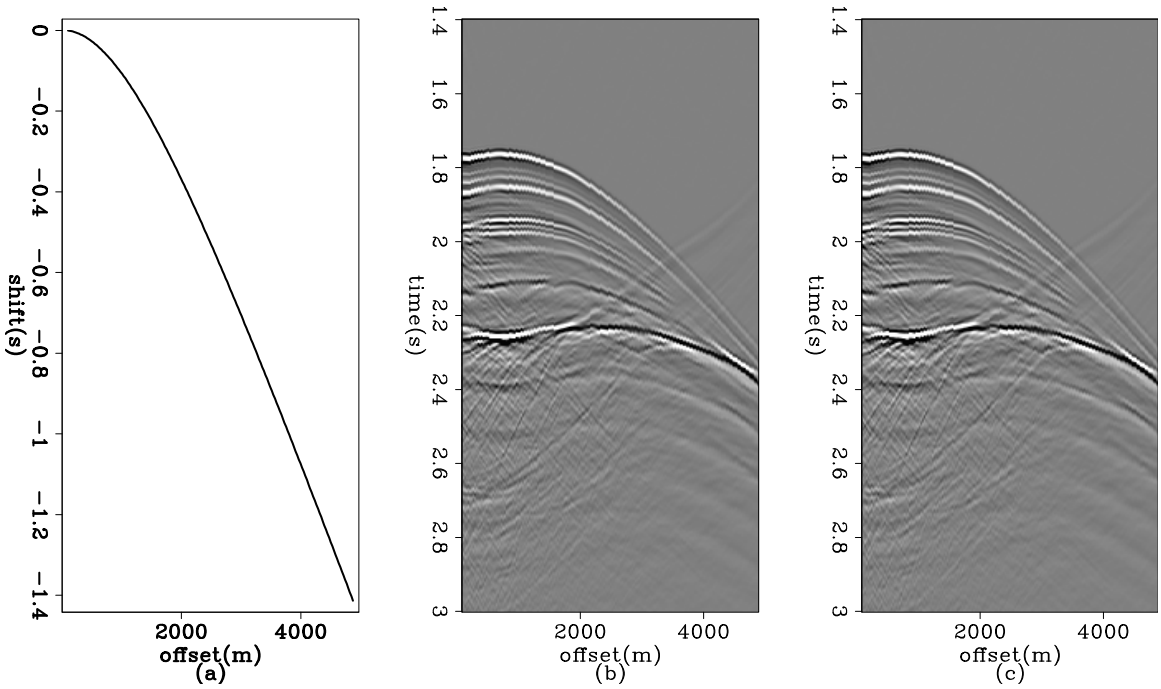

Figure 9: (a)The time shift function to flatten the gather; (b) and (c) two shifted shot gathers. [**ER**]

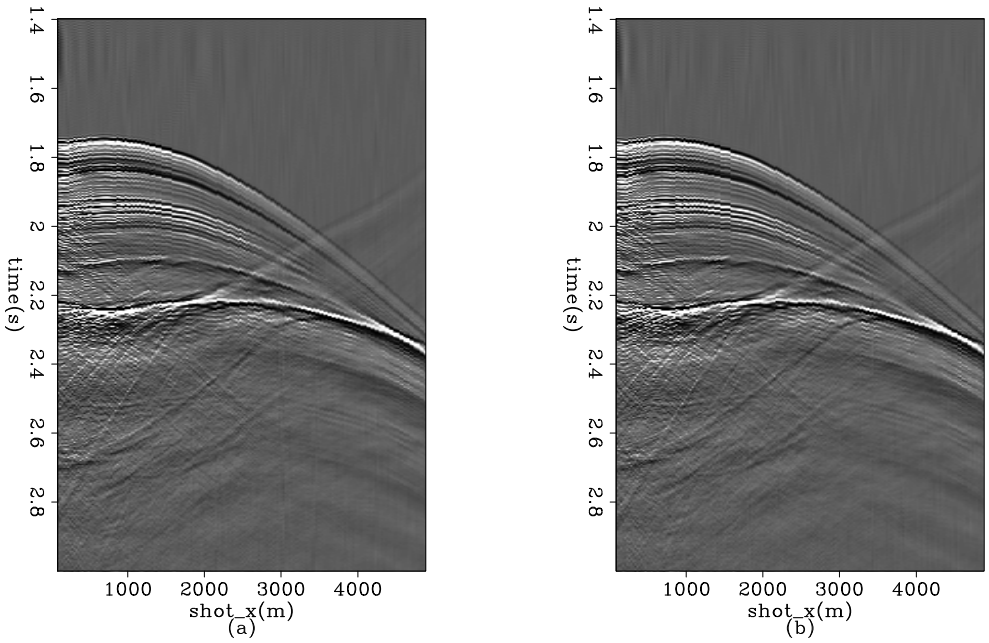

Figure 10: Two shot gathers after applying Burg PEF preconditioning. Different PEF filters are estimated and applied separately. [**ER**]

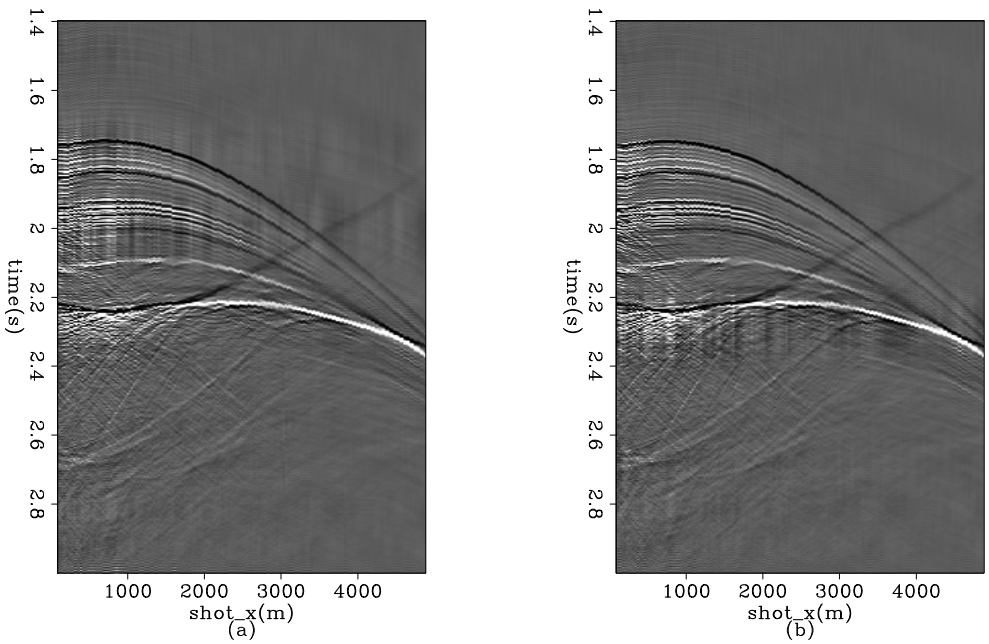

Figure 11: Two shot gathers after logarithm Fourier domain bidirectional deconvolution. The deconvolution is applied separately for each gather and within the same shot gather we use one costant deconvolution filter for all traces [**ER**]

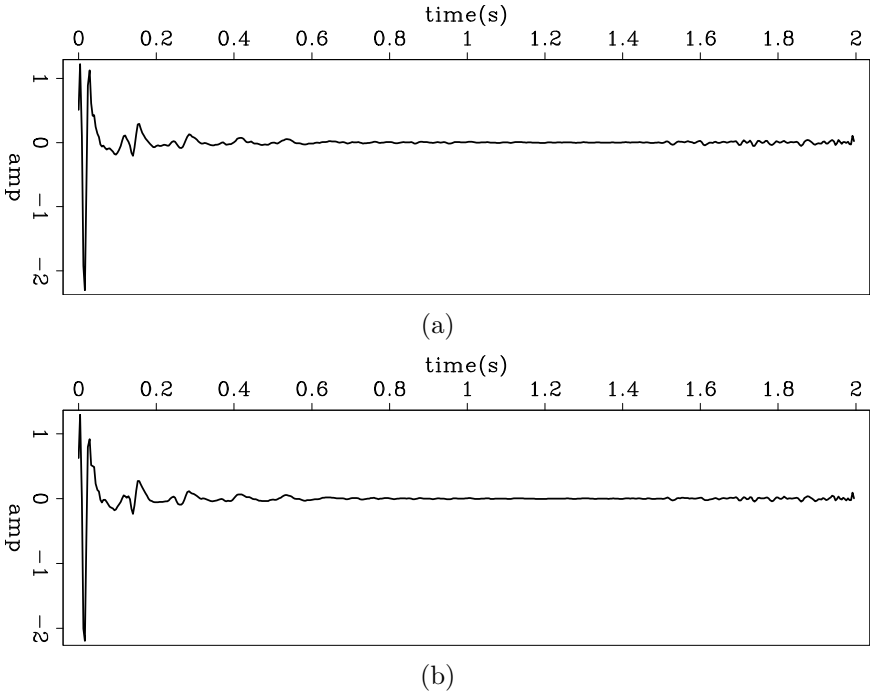

Figure 12: The estimated wavelets by logarithm Fourier-domain bidirectional deconvolution. (a) Shot gather 14000; (b) shot gather 14028. We notice that the in the Ricker part, (b) is less symmetric than (a), but we do not know exactly what cause this difference. [**ER**]

We also tried deconvolution of multi-shot gathers with one filter. Figures 13 and 14 show deconvolution results for 39 and 451 shot gathers, respectively, and figures 15(a), 15(b) and 15(c) show a comparison among estimated wavelets of single shot gathers and multi-shot gathers. The wavelets are similar, and from panels (a) to (c) we can see that using more shot gathers reduces jitter. These results tell us that the shot waveforms do not change significantly from shot to shot. This is consistent with our observations in the previous analysis of two shot gathers.

we notice in the figure 15(c), there is low frequency component which looks like a white stripe within the salt body. We do not have the similar thing in our common offset result (figure 4). We expect to get better deconvolution quality for pre-stack gathers due to we have more data, but the results show us the oppsite conclusion. That is a indicate the wavelet is various with offset changing. We need a way to use various wavelet for different offset range to handle this problem. But we can not simply divided the shot gathers into several vertical stripes because the wavelet is function of both offset and travel time (and maybe tavelling angle). We need more work to find out the pattern to separate shot gather into portions in which one portion has a relative constant wavelet. Furthermore, we also need to figure out the suitable gain function as the weighting for bidirectional deconvolution before we do more test on this pre-stack data set.

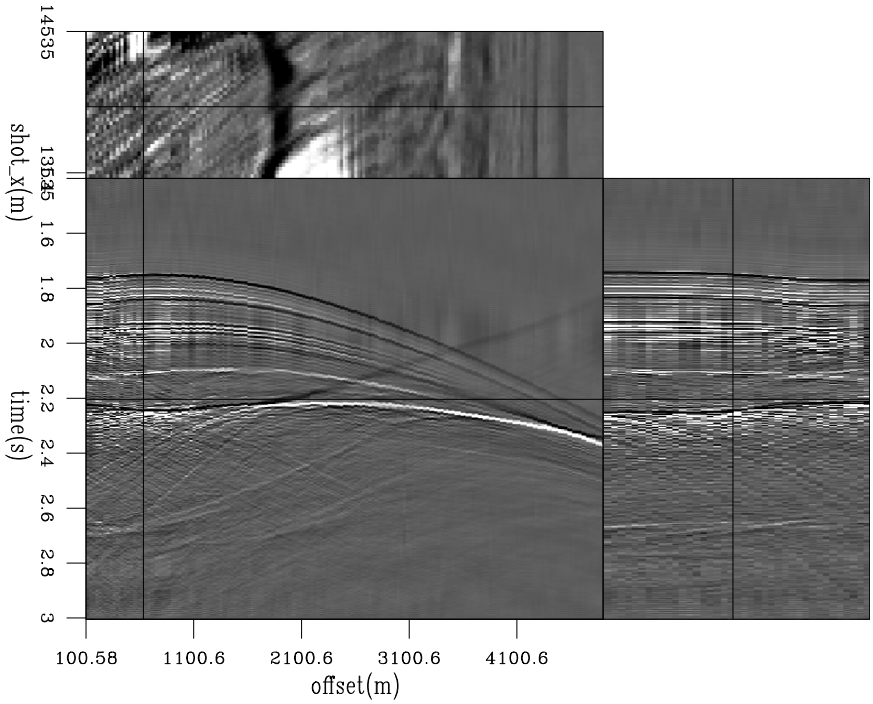

Figure 13: Logarithm Fourier-domain bidirectional deconvolution result on 39 shot gathers. [**ER**]

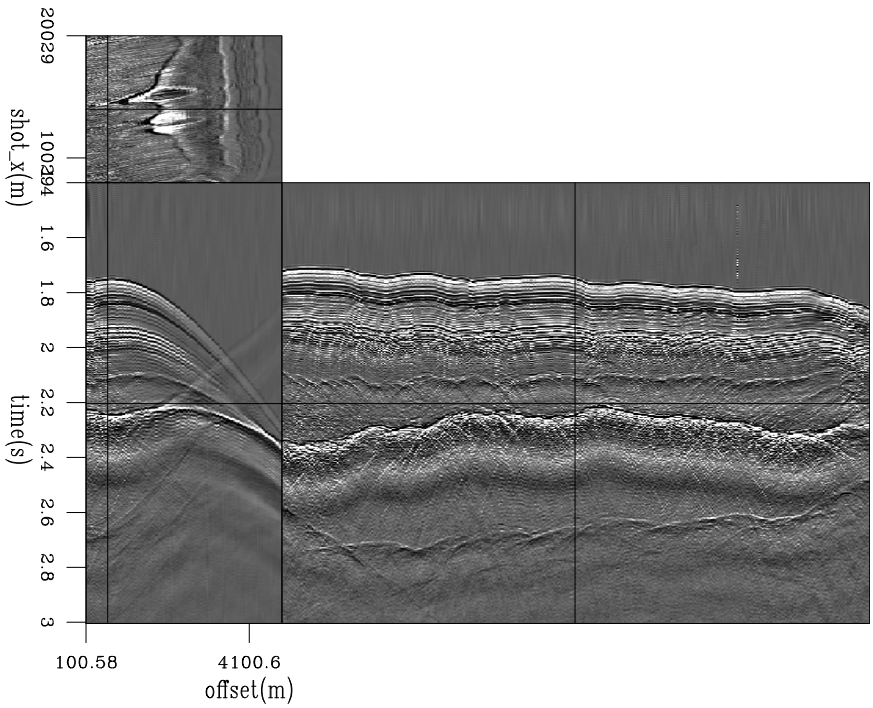

Figure 14: Logarithm Fourier-domain bidirectional deconvolution result on 451 shot gathers. [**CR**]

ACKNOWLEDGMENTS

We would like to thank Yang Zhang, Shuki Ronen, Robert Clapp, Dave Nichols and Antoine Guitton for helpful discussions of our research.

REFERENCES

Claerbout, J., 2009, Blocky models via the l1/l2 hybrid norm: SEP-Report, **139**, 1–10.

Claerbout, J., Q. Fu, and Y. Shen, 2011, A log spectral approach to bidirectional deconvolution: SEP-Report, **143**, 297–300.

Fu, Q., Y. Shen, and J. Claerbout, 2011, An approximation of the inverse ricker wavelet as an initial guess for bidirectional deconvolution: SEP-Report, **143**, 283–296.

Shen, Y., Q. Fu, and J. Claerbout, 2011a, A new algorithm for bidirectional deconvolution: SEP-Report, **143**, 271–282.

———, 2011b, Preconditioning a non-linear problem and its application to bidirectional deconvolution: SEP-Report, **145**, 117–130.

Zhang, Y. and J. Claerbout, 2010a, Least-squares imaging and deconvolution using the hb norm conjugate-direction solver: SEP-Report, **140**, 129–142.

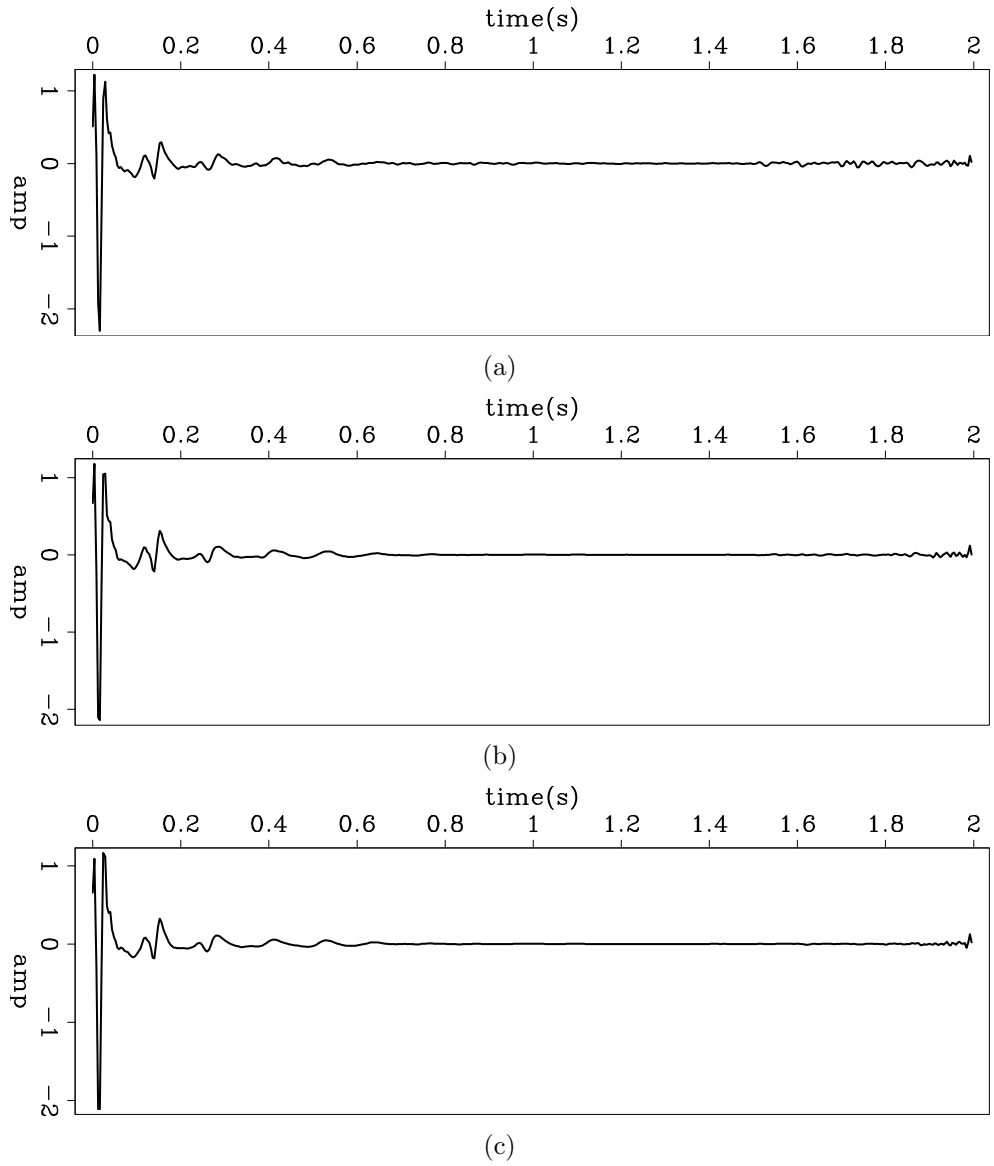

Figure 15: The wavelets estimated from (a) one shot gather (same as 12(a)); (b) 39 shot gathers (from shot location of 13500 meters to 14500 meters); (c) 451 shot gathers (from shot location of 8000 meters to 20000 meters). [**ER**]

———, 2010b, A new bidirectional deconvolution method that overcomes the minimum phase assumption: SEP-Report, **142**, 93–104.